Hindawi
International Journal of Antennas and Propagation
Volume 2021, Article ID 9966495, 9 pages
https://doi.org/10.1155/2021/9966495

Research Article

A New Wideband Circularly Polarized Dielectric Resonator Antenna Loaded with Strips

Lichao Hao,[1,2] **Hao Wang**,[3] **Bo Li**,[4] **and Wenting Yin**[5]

[1]*Huada Semiconductor Co., Ltd, Shanghai, China*
[2]*School of Microelectronics, Guangdong University of Technology, Guangzhou, China*
[3]*China Academy of Information and Communications Technology, The Research Institute of Informatization and Industrialization Integration, Beijing, China*
[4]*China Electronics Corporation, Beijing, China*
[5]*Empyrean Technology Co., Ltd, Beijing, China*

Correspondence should be addressed to Hao Wang; wanghao1@caict.ac.cn and Wenting Yin; yinwt@empyrean.com.cn

Received 16 March 2021; Revised 11 May 2021; Accepted 17 June 2021; Published 5 July 2021

Academic Editor: Renato Cicchetti

This paper proposes a novel wideband circularly polarized (CP) dielectric resonator antenna (DRA) loaded with strips. The CP DRA comprises a circular DR, two pairs of driven L-like DR strips with different lengths, and a square ground-plane. To couple the electromagnetic energy to circular DR, an orthogonal cross-slot is used, and a stepped microstrip-line is also used to adjust the impedance matching. Influenced by the concept of deformed DR, two pairs of L-like DR strips of different lengths are inserted into the circular DR as part of the driven element to excite a new axial ratio (AR) resonant point. An antenna prototype is simulated, manufactured, and measured to validate the unique design. The measured results show that the designed antenna has broadband characteristic with a −10 dB IBW of 54% (1.91–3.32 GHz) and 3 dB ARBW of 42.1% (2.10–3.22 GHz).

1. Introduction

Recently, DRAs [1, 2] have been intensively studied due to the attractive features of high efficiency, low cost, and wideband operation. The basic characteristics of DRAs in higher-order mode, CP dual-function and transparent designs, and a glass decoration DRA are described in [1] for the first time. In [2], a novel high-gain mushroom-shaped DRA was designed to obtain −10 dB impedance bandwidth (IBW) of 65%, which comprises a hollow cylindrical resonator and a top-mount spherical-cap lens used to increase the gain. Compared with linearly polarized DRAs, CP DRAs [3, 4] with the advantages of mitigating multipath fading and polarization mismatch have become increasingly common in wireless communication systems. However, the bandwidth of CP DRAs is typically insufficient to satisfy the needs of broadband communication.

Various feeding methods have been presented in [5–17] to realize the broadband CP radiation. The CP DRAs are summarized as multiple-feeding and single-feeding structures. Although the multiple-feeding DRAs can easily achieve a wideband CP compared with the single-feeding DRAs, it requires additional hybrid-couplers or power-dividers [5–9], which inevitably increases the antenna dimension and structure complexity. Therefore, studying broadband CP DRAs with single-feeding characteristics is a great challenge and potentiality recently.

Several single-feeding structures are presented in [10–17] to increase the bandwidth of single-feeding CP DRAs, such as deformed microstrip feeding [10], coaxial-probe feeding [11], modified cross-slot feeding [12], asymmetrical U-slot [13], monofilar-spiral slot [14], and Archimedean spiral slot [15]. Except for using different single-feeding structures, various DR shapes [18–25], such as multiple-circular-sector [18], pixelated [19], and spidron-fractal shapes [20], have also been designed to increase the CP bandwidth (CPBW) of DRAs. Rectangular and cylindrical rings and hemispherical DRs are introduced sequentially in [23–25], which can

obtain 27.7%, 6.4%, and 3.9% 3 dB axial ratio bandwidth (ARBW), respectively. The use of parasitic branches [26–28] is also emphasized as an effective way to improve the CPBW of single-feeding DRAs. Wideband CP performance was realized in [26, 27] by loading four rotated metallic plates and a partially reflective surface into square DR with a cross-slot coupled feeding structure, which achieves 49.5% and 54.9% 3 dB ARBW, respectively. Similarly, two half-ring DRs are inserted in [28] to stimulate an additional AR resonant point, which can gain a wide CPBW of 46.8%.

Influenced by the concept of deformed DR, in this study, two pairs of driven L-like DR strips of different lengths are introduced into a circular DR as part of the driven element for enhancing the CPBW. An orthogonal cross-slot is used to couple the electromagnetic energy to circular DR, and a stepped microstrip-line is used to adjust the impedance matching. First, the circular DR is used to achieve broad CP operation through a cross-slot coupled method. Second, two pairs of driven L-like DR strips of different lengths are placed next to the circular DR, which can jointly stimulate a high-frequency additional AR resonant. Third, by optimizing and using these structures, the proposed DRA's IBW and ARBW are widened. Finally, to demonstrate the wideband CP design concept, an optimized antenna prototype is simulated, fabricated, and measured. The measured results show that the designed CP DRA exhibits a wide characteristic of 54%–(1.91–3.32 GHz–) 10 dB IBW, and 42.1% (2.10–3.22 GHz) 3 dB ARBW, which has potential application values in wireless local area network (WLAN, 2.4–2.48 GHz) and wireless broadband access service (WiBro, 2.3–2.39 GHz) communication systems. The corresponding content is summarized in four sections to explain the operated mechanism. Section 1 shows the introduction; Section 2 is the description of the antenna structure and the principle analysis of designed process; Section 3 compares measured and simulated results, and Section 4 concludes the feature of the proposed antenna.

2. Antenna Design

2.1. Antenna Configuration. Figure 1 shows the structure and dimensions of the designed CP DRA. As shown, the antenna consists of a circular DR ($R1$), two pairs of driven L-like DR strips ($R2 \times W5$, $R3 \times W6$), a square ground-plane ($L \times W$), and a stepped microstrip-line ($L1 \times W1$, $L2 \times W2$). The circular DR and DR strips with the same height ($H2 = 19$ mm) and dielectric constant ($\varepsilon r_2 = 10.2$) are placed on top of an FR4-substrate with permittivity ($\varepsilon r_1 = 4.4$) and height ($H1 = 0.8$ mm). The stepped microstrip-line is placed on the bottom surface of the FR4-substrate to improve impedance matching. Additionally, an orthogonal cross-slot of different sizes ($L3 \times W3$, $L4 \times W4$) is etched into the square ground to provide the original CP mode. Because of the introduction of the L-like DRs, the CPBW can be expanded, and a new AR passband in high frequency is excited. Table 1 shows the detailed parameter values optimized by using an electromagnetic simulator (ANSYS HFSS).

2.2. Antenna Mechanism. Figure 2 shows four step-by-step antenna's prototypes used to elaborate the broadband CP operating principle. Ant. 1 is a typical circular DR with cross-slot coupled feeding; Ant. 2 inserts a pair of driven L-like DR strips with an arc of $\theta 3$; Ant. 3 introduces a pair of driven L-like DR strips with an arc of $\theta 2$. By integrating these driven DR strips, the CP DRA is designed. The corresponding variations of IBW and ARBW with four evolutionary prototypes are *pl*otted in Figure 3. Two CP resonant modes of Ant. 1 are excited at 2.20 and 2.86 GHz, respectively. Generally, when an orthogonal cross-slot is used as a coupled feeding structure and is placed in a circular or square DR, two pairs of orthogonal modes can be excited, as discussed and analyzed in [26]. The low-frequency AR point (2.20 GHz) comes from the interaction between TE_{111} ($x1$) and TE_{111} ($y1$) modes of DRA, whereas the high-frequency AR point (2.86 GHz) is excited by the x'-polarized mode of short slot and the TE_{111} ($y1$) mode of DRA, as shown in Figure 3(b). Without adding any DR strips, the optimal bandwidth of Ant. 1 is too narrow to meet the communication requirements. Two pairs of driven L-like DR strips with different arcs of $\theta 2$ and $\theta 3$ are introduced into Ant. 2 and Ant. 3 to increase the CPBW. As shown, these driven L-like DR strips can not only improve IBW but also reduce the AR values. It is noticed that the L-like DR strips with an arc of $\theta 2$ have a significant impact on the CPBW than L-like DR strips with an arc of $\theta 3$. When two pairs of driven L-like DR strips are integrated and placed next to the circular DR, an AR resonant point at 3.16 GHz can be stimulated. Furthermore, the ARBW shifts toward higher frequencies and the IBW and ARBW in lower frequencies could also be improved. After simulating and optimizing, the presented antenna exhibits a −10 dB IBW of 49.6% (2.00–3.32 GHz) and 3 dB ARBW of 43.6% (2.08–3.24 GHz).

2.3. Electric Field Distribution. The vector electric filed distributions on the upper surface of circular DR and L-like DR strips are simulated at 2.18, 2.72, and 3.16 GHz to clarify the DRA's CP operating principle, as shown in Figure 4. All the simulated results are produced by commercial software ANSYS Electronics Desktop. The input power is 1 W, and a 50 Ω lumped port is also used to excite the proposed CP DRA. As shown in Figures 4(a) and 4(b), the electric field mainly concentrates on the circular DR at 2.18 and 2.72 GHz. The electric filed direction of the circular DR and L-like DR strips is the same, and the vector electric fields at phase = 0° and 90° are orthogonal. However, at 3.16 GHz, the electric field of L-like DR strips and the partial electric field of the circular DR are reverse and cancel each other out. In addition, the vector electric field at phase = 0° and 90° is also orthogonal at 3.16 GHz. With the different phases (0° and 90°), the direction of the vector electric field rotates clockwise at three frequency points, which means the proposed CP DRA can radiate left-hand CP waves. Finally, the designed DRA's CPBW can be significantly enhanced by combining these CP resonant points.

2.4. Antenna Parameter Analysis. To study the influence of antenna dimensions on CPBW, some parameters are scanned and analyzed in this section. The arcs of L-like DR

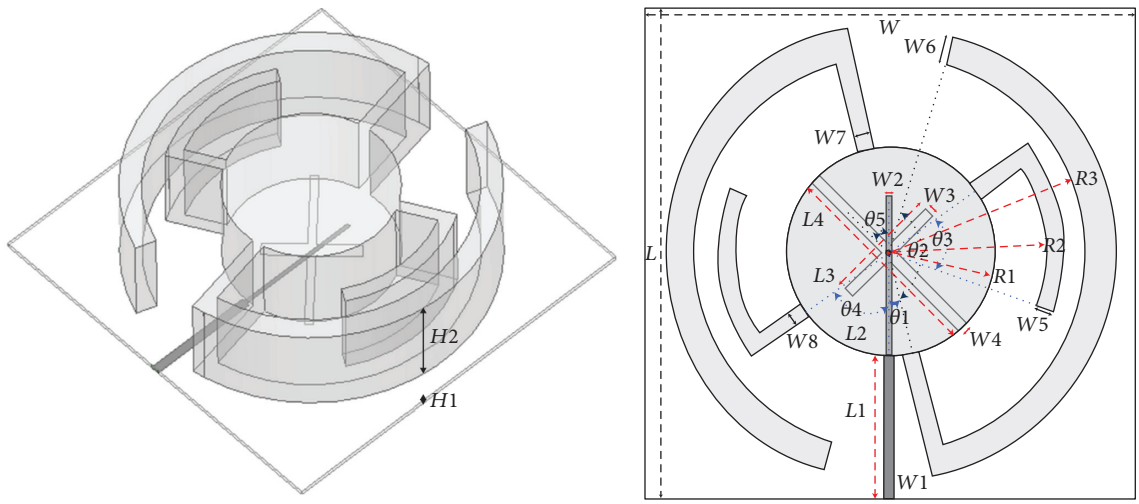

Figure 1: The structure of the presented CP DRA.

Table 1: The geometrical parameters.

Sizes	Values
L	76 mm
$L1$	22 mm
$L2$	25 mm
$L3$	18 mm
$L4$	33 mm
W	76 mm
$W1$	1.8 mm
$W2$	0.8 mm
$W3$	2.6 mm
$W4$	1.5 mm
$W5$	2.8 mm
$W6$	4.0 mm
$W7$	2.4 mm
$W8$	2.2 mm
$R1$	16 mm
$R2$	23.8 mm
$R3$	30 mm
$H1$	0.8 mm
$H2$	19 mm
$\theta1$	11°
$\theta2$	150°
$\theta3$	60°
$\theta4$	60°
$\theta5$	45°

strips ($\theta2$ and $\theta3$), the width of the stepped microstrip-line ($W1$), and the width of the orthogonal cross-slot ($W3$) are analyzed using simulated soft ANSYS HFSS. The corresponding 3 dB ARBW and −10 dB IBW with different sizes are shown in Figure 5. Note that the IBW varies significantly with different $W3$ and $W1$ values across the whole operating bandwidth, whereas the AR values barely vary. This means that the two parameters are crucial in controlling the proposed antenna's impedance matching. However, compared with $W1$ and $W3$, the AR values change significantly with different arcs of $\theta2$ and $\theta3$. Furthermore, the $|S_{11}|$ values vary in the whole frequency band. Therefore, the L-like DR strips also participate in the excitation of CP mode. The best $|S_{11}|$ and AR values were obtained when $W1 = 1.8$ mm, $W3 = 2.6$ mm, $\theta2 = 150°$, and $\theta3 = 60°$. Additionally, Table 2 compares the previously published and presented CP DRAs, revealing that the designed antenna with modified DR has an excellent CPBW. In addition, although the [26–28] have more compact and higher CPBW than the proposed antenna, the proposed CP DRA design is unique, and their bandwidth enhancement methods are completely different. The bandwidths of [26–28] are increased by introducing parasitic elements, whereas the proposed antenna is enhanced by loading modified DR.

3. Experimental Results

In this section, an optimal antenna's prototype is manufactured and measured to verify the design accuracy. The −10 dB reflection coefficients ($|S_{11}|$) are tested using vector network analyser (Agilent N5224A), and an anechoic chamber is used to measure the gains, ARs, and radiation patterns. To show a clear comparison, the correspondingly tested and simulated results are shown in Figures 6–8. As shown, the measured and simulated −10 dB IBW is 54% (1.91–3.32 GHz) and 49.6% (2.00–3.32 GHz), whereas the 3 dB ARBW is 42.1% (2.10–3.22 GHz) and 43.6% (2.08–3.24 GHz), separately. Note that the measured −10 dB IBW completely covers the whole 3 dB ARBW, implying that usable overlapping bandwidth is more than 42%. Furthermore, within the CPBW, the tested and simulated peak gains are approximately 5.92 and 6.18 dBic, respectively. The simulated radiation efficiency is greater than 95%. A notch appears at 2.4 GHz in the |S11| and gain curves, which could be caused by the interaction between cross-slot and microstrip-line. Furthermore, Figure 7 includes measured photograph of the designed antenna. The normalized radiation patterns of the prototype in two orthogonal planes (phi = 0° and 90°) with different frequencies (2.18, 2.72, and 3.16 GHz) are plotted in Figure 8. As depicted, left-hand CP fields are stronger than the right-hand CP parts by more than 25 dB, which means the LHCP waves can be radiated at three frequency points in $+z$-direction. At certain

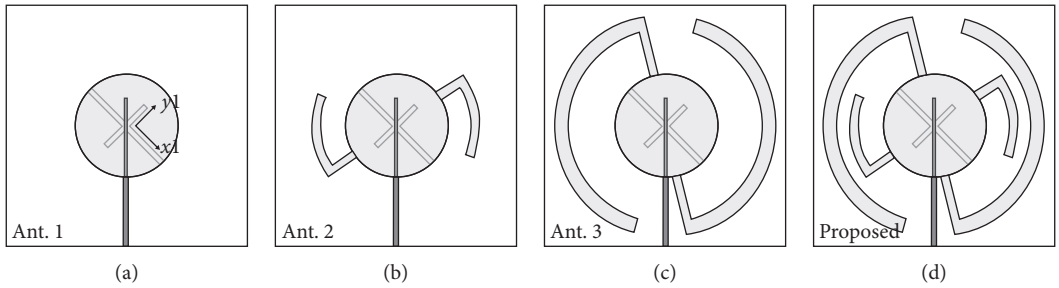

Figure 2: Four antenna prototypes in the design process.

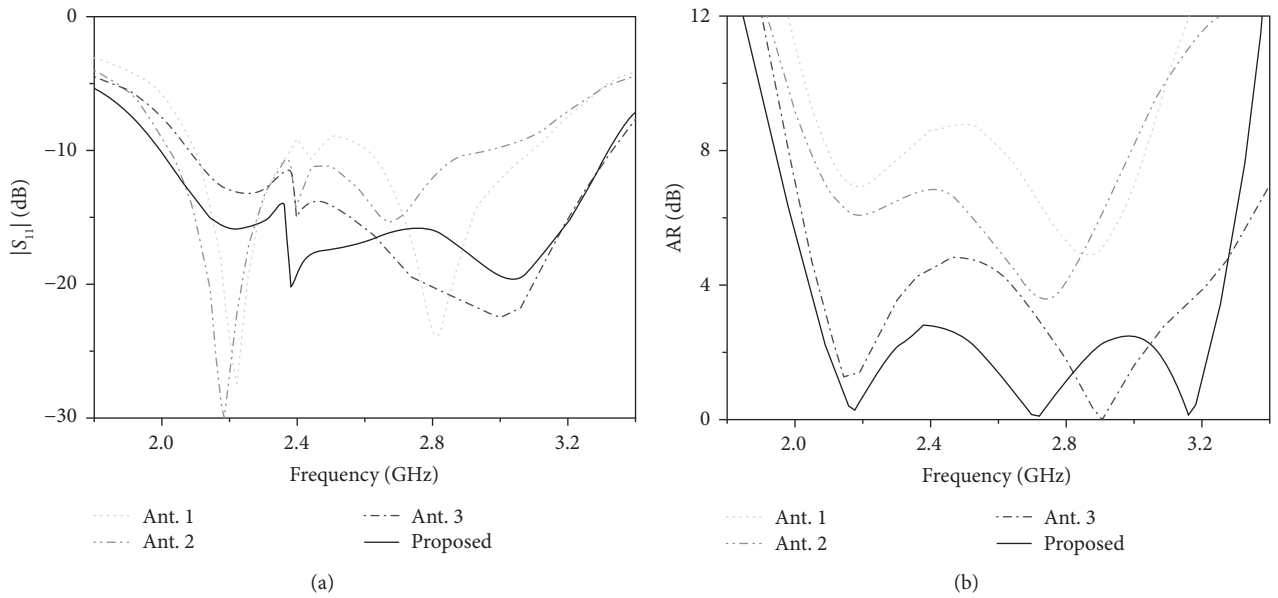

Figure 3: |S11| and AR curves for different antennas: (a) $|S_{11}|$ curves and (b) AR curves.

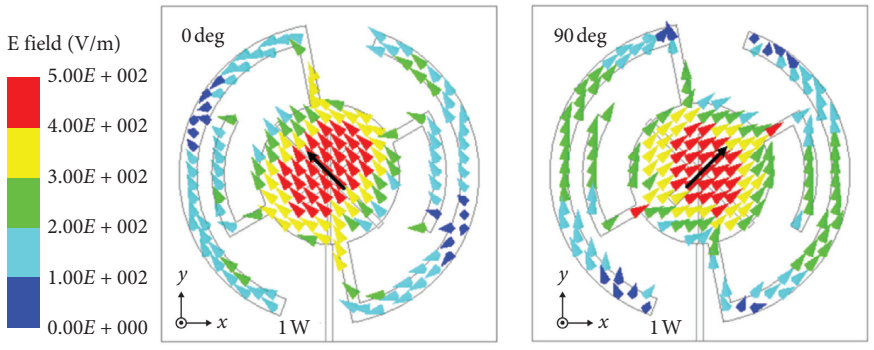

Figure 4: Continued.

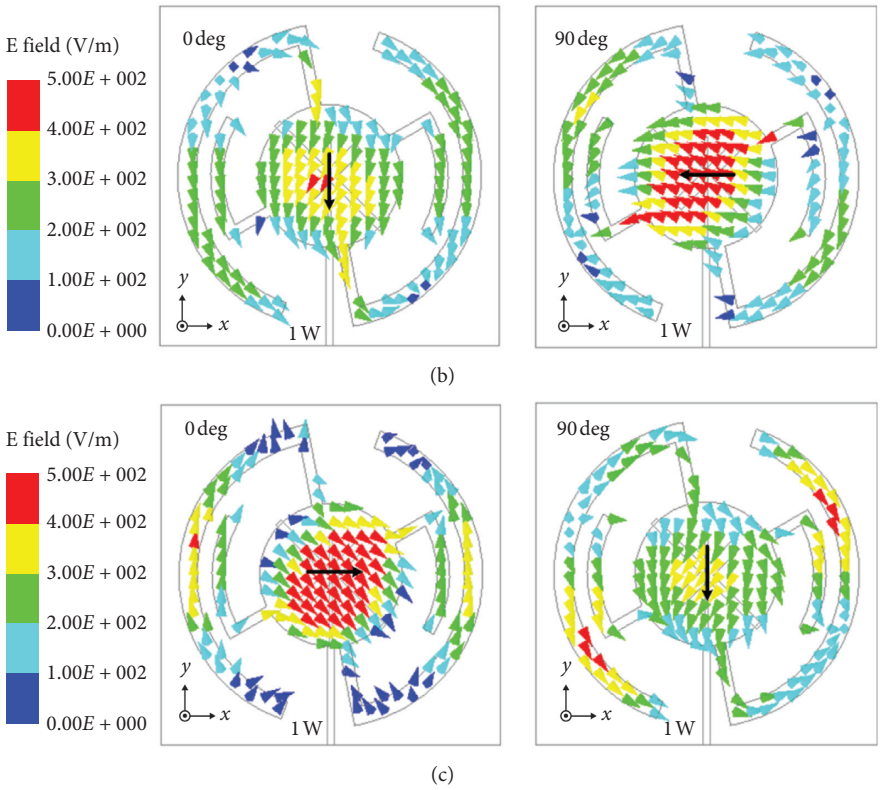

Figure 4: Simulated vector electric field distributions on the upper surface of DR with different phases of 0° and 90°at (a) 2.18 GHz, (b) 2.72 GHz, and (c) 3.16 GHz, respectively.

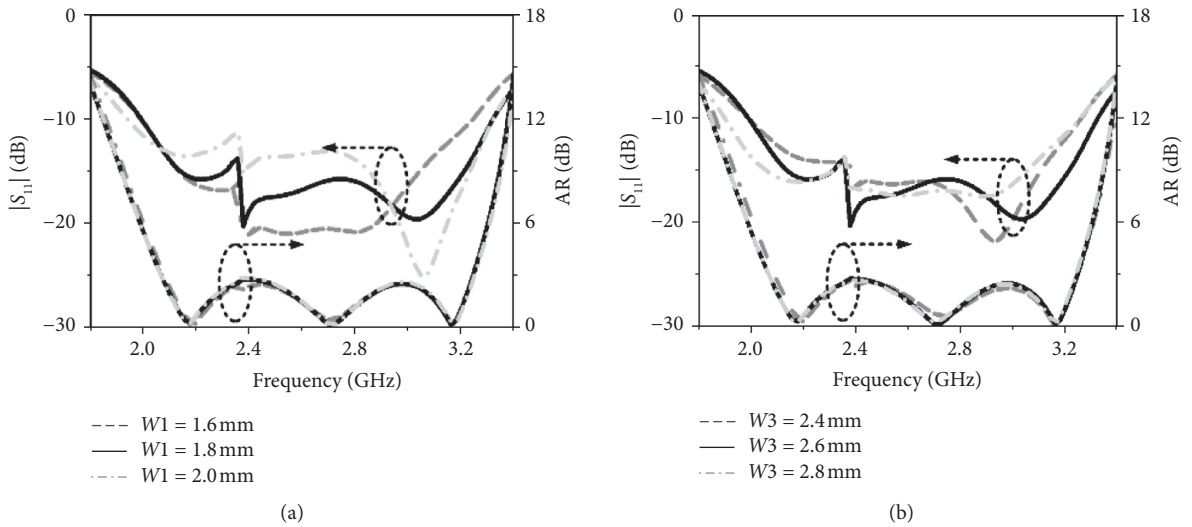

Figure 5: Continued.

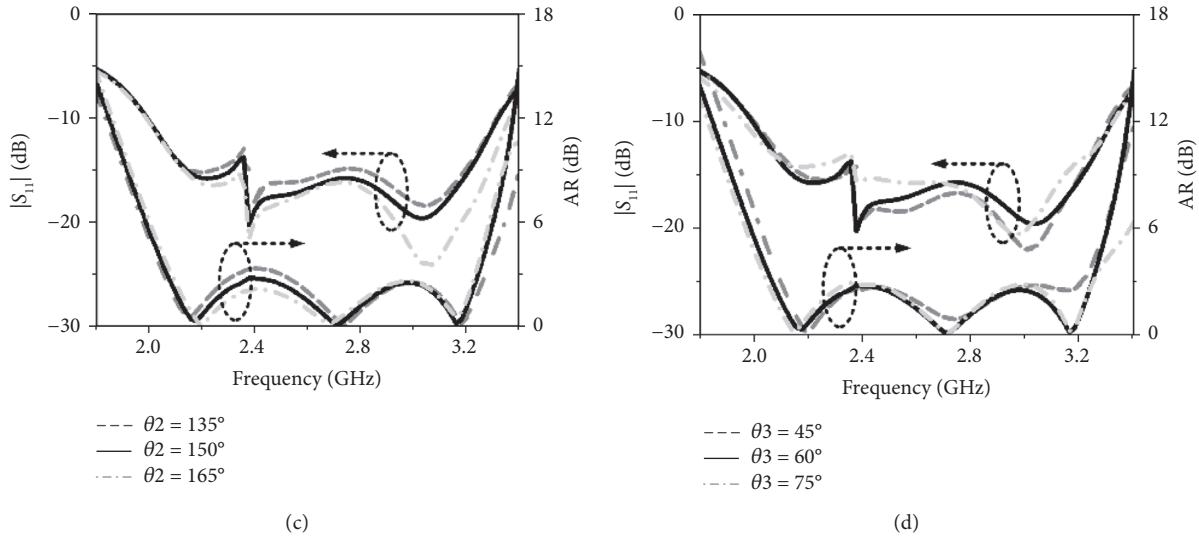

Figure 5: $|S_{11}|$ and AR curves of the designed antenna with different parameters: (a) $W1$, (b) $W3$, (c) $\theta 2$, and (d) $\theta 3$.

Table 2: Comparison of the designed antenna with previously reported antennas

Ref. Antenna	Type	Antenna size (λ_0^3)	−10 dB IBW (%)	3 dB ARBW (%)	Overlapping BW (%)	Peak gain (dBic)
[15]	Using Archimedean spiral slot	$0.56 \times 0.56 \times 0.09$	NA	25.5	25.5	5.0
[17]	Joining two rectangular DRs	$0.98 \times 0.98 \times 0.26$	37.0	22.0	22.0	5.7
[21]	Using trapezoidal DR	$1.20 \times 1.20 \times 0.45$	34.6	20.4	20.4	8.4
[26]	Using parasitic vertical plates	$0.72 \times 0.72 \times 0.18$	46.9	49.5	46.9	4.7
[27]	Using partially reflective surface	$1.38 \times 1.38 \times 0.60$	54.3	54.9	54.1	14.2
[28]	Using two parasitic half-ring DRs	$0.76 \times 0.76 \times 0.20$	52.2	46.8	46.8	5.7
Proposed	Using two pairs of driven L-like DR strips	$\mathbf{0.76 \times 0.76 \times 0.20}$	**54**	**42.1**	**42.1**	**5.92**

λ_0 is the free space wavelength at the center frequency of the overlapped band.

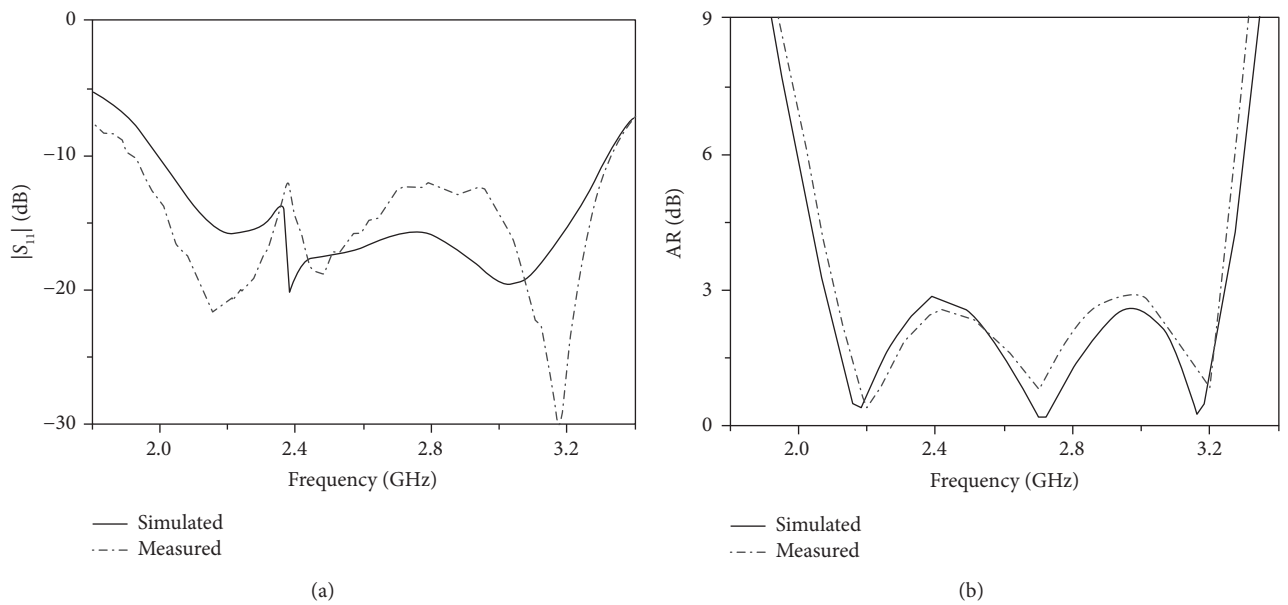

Figure 6: (a) $|S_{11}|$ and (b) AR curves of simulated and tested antenna prototype.

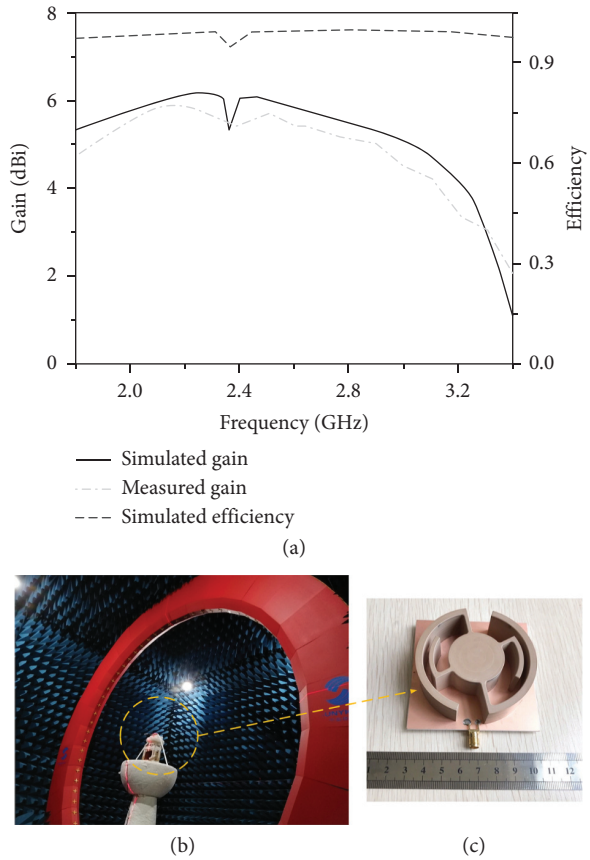

Figure 7: (a) Measured and simulated antenna gains, (b) simulated radiation efficiency, (c) and the photograph of the measurement environment as well as antenna prototype.

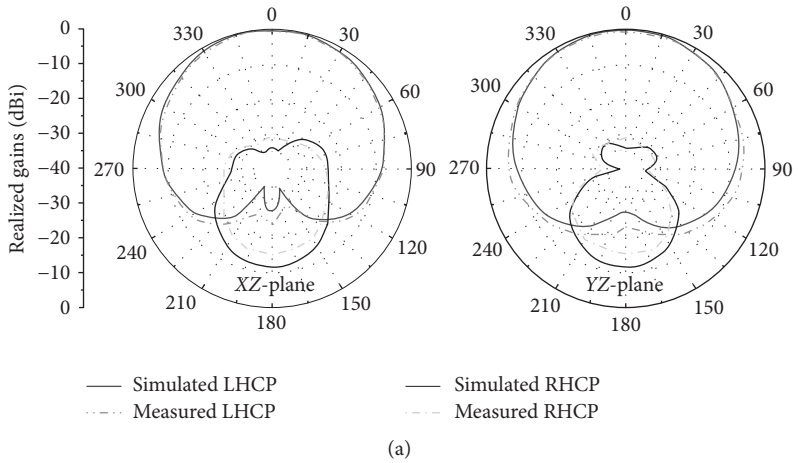

Figure 8: Continued.

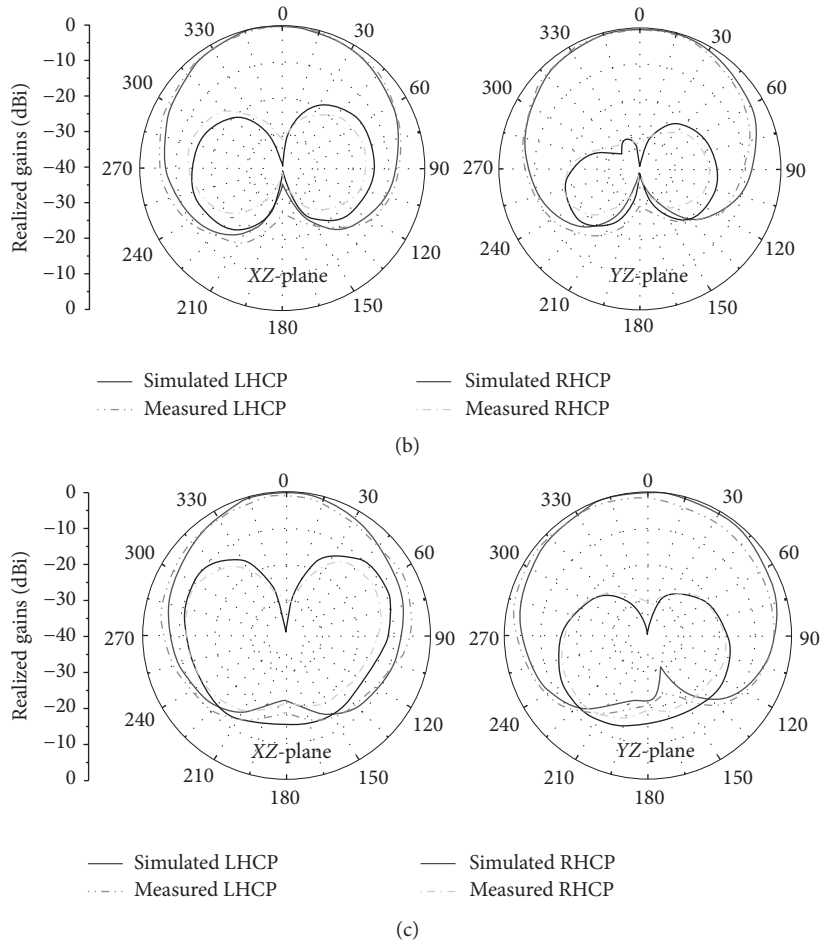

Figure 8: Simulated and tested normalized radiation patterns of the designed antenna at (a) 2.18, (b) 2.72 GHz, and (c) 3.16 GHz.

frequencies, the front-to-back ratios of the proposed antenna are below −20 dB, indicating that the antenna produces a higher front-to-back ratio. There is a slight mismatch between the simulated and measured results because of the imperfect fabricated and tested environment. Finally, the rationality of the prototype can be verified by combining these simulated and tested results.

4. Conclusion

This paper proposes a new wideband CP DRA loaded with strips. The DRA comprises a circular DR, two pairs of driven L-like DR strips of different lengths, and a square groundplane. An orthogonal cross-slot is used to couple the electromagnetic energy to the circular DR, and a stepped microstrip-line is used to improve IBW. Influenced by the concept of deformed DR, two pairs of L-like DR strips of different lengths are inserted into the circular DR as part of the driven element to excite a new AR resonant point. To verify the design, a prototype of the designed DRA is fabricated and measured. The measured results show that the CP DRA has a wider 3 dB ARBW of 42.1% (2.10–3.22 GHz) and a broader −10 dB IBW of 54% (1.91–3.32 GHz), indicating that the CP DRA has potential applications for wireless local area network (WLAN, 2.4–2.48 GHz), wireless broadband access service (WiBro, 2.3–2.39 GHz), and world interoperability for microwave access (WiMAX, 2.5–2.7 GHz) communication systems.

Data Availability

The data used to support the findings of this study are available from the corresponding author upon request.

Conflicts of Interest

The authors declare that they have no conflicts of interest.

References

[1] K. W. Leung, E. H. Lim, and X. S. Fang, "Dielectric resonator antennas: from the basic to the aesthetic," *Proceedings of the IEEE*, vol. 100, no. 7, pp. 2181–2193, 2012.

[2] R. Cicchetti, A. Faraone, E. Miozzi, R. Ravanelli, and O. Testa, "A high-gain mushroom-shaped dielectric resonator antenna for wideband wireless applications," *IEEE Transactions on Antennas and Propagation*, vol. 64, no. 7, pp. 2848–2861, 2016.

[3] R. K. Mongia and P. Bhartia, "Dielectric resonator antennas-a review and general design relations for resonant frequency and bandwidth," *International Journal of RF and Microwave Computer-Aided Engineering*, vol. 4, no. 3, pp. 230–247, 1994.

[4] M. B. Oliver, Y. M. M. Antar, R. K. Mongia, and A. Ittipiboo, "Circularly polarised rectangular dielectric resonator antenna," *Electronics Letters*, vol. 31, no. 6, pp. 418-419, 1995.

[5] A. A. Kishk, "Application of rotated sequential feeding for circular polarization bandwidth enhancement of planar arrays with single-fed DRA elements," *Proceedings of IEEE Antennas and Propagation Society International Symposium*, vol. 4, pp. 664–667, 2003.

[6] G. Massie, M. Caillet, M. Clénet, and Y. M. M. Antar, "A new wideband circularly polarized hybrid dielectric resonator antenna," *IEEE Antennas and Wireless Propagation Letters*, vol. 9, pp. 347–350, 2010.

[7] B. Rana and S. K. Parui, "Microstrip line fed wideband circularly-polarized dielectric resonator antenna array for microwave image sensing," *IEEE Sensors Letters*, vol. 1, no. 3, pp. 1–4, 2017.

[8] R. C. Han, S. S. Zhong, and J. Liu, "Broadband circularly polarized dielectric resonator antenna fed by wideband switched line coupler," *Electronics Letters*, vol. 50, no. 10, pp. 725-726, 2014.

[9] S. K. Podilchak, J. C. Johnstone, M. Caillet, M. Clénet, and Y. M. M. Antar, "A compact wideband dielectric resonator antenna with a meandered slot ring and cavity backing," *IEEE Antennas and Wireless Propagation Letters*, vol. 15, pp. 909–913, 2016.

[10] R. Kumar and R. K. Chaudhary, "A wideband circularly polarized cubic dielectric resonator antenna excited with modified microstrip feed," *IEEE Antennas and Wireless Propagation Letters*, vol. 15, pp. 1285–1288, 2016.

[11] P. Patel, B. Mukherjee, and J. Mukherjee, "Wideband circularly polarized rectangular dielectric resonator antennas using square-shaped slots," *IEEE Antennas and Wireless Propagation Letters*, vol. 15, pp. 1309–1312, 2016.

[12] M. Zou and J. Pan, "Wideband hybrid circularly polarised rectangular dielectric resonator antenna excited by modified cross-slot," *Electronics Letters*, vol. 50, no. 16, pp. 1123–1125, 2014.

[13] B. Li, K. K. So, and K. W. Leung, "A circularly polarized dielectric resonator antenna excited by an asymmetrical U-slot with a backing cavity," *IEEE Antennas and Wireless Propagation Letters*, vol. 2, pp. 133–135, 2003.

[14] M. Zou, J. Pan, and Z. Nie, "A wideband circularly polarized rectangular dielectric resonator antenna excited by a lumped resistively loaded monofilar-spiral-slot," *IEEE Antennas and Wireless Propagation Letters*, vol. 12, pp. 1646–1649, 2013.

[15] M. Zou, J. Pan, and Z. Nie, "A wideband circularly polarized rectangular dielectric resonator antenna excited by an Archimedean spiral slot," *IEEE Antennas and Wireless Propagation Letters*, vol. 14, pp. 446–449, 2015.

[16] K. W. Khoo, Y. X. Guo, and L. C. Ong, "Wideband circularly polarized dielectric resonator antenna," *IEEE Antennas and Wireless Propagation Letters*, vol. 55, no. 7, pp. 1929–1932, 2007.

[17] S. Fakhte, H. Oraizi, R. Karimian, and R. Fakhte, "A new wideband circularly polarized stair-shaped dielectric resonator antenna," *IEEE Transactions on Antennas and Propagation*, vol. 63, no. 4, pp. 1828–1832, 2015.

[18] T. V. Son, "A wideband circularly polarized antenna with a multiple-circular-sector dielectric resonator," *Sensors*, vol. 16, no. 11, p. 1849, 2016.

[19] S. Trinh-Van, Y. Yang, K.-Y. Lee, and C. K. Hwang, "A wideband circularly polarized pixelated dielectric resonator antenna," *Sensors*, vol. 16, no. 9, p. 1349, 2016.

[20] A. Altaf, Y. Yang, K. Lee, and K. C. Hwang, "Circularly polarized spidron fractal dielectric resonator antenna," *IEEE Antennas and Wireless Propagation Letters*, vol. 14, pp. 1806–1809, 2015.

[21] Y. M. Pan and K. W. Leung, "Wideband circularly polarized trapezoidal dielectric resonator antenna," *IEEE Antennas and Wireless Propagation Letters*, vol. 9, pp. 588–591, 2010.

[22] Y. M. Pan and K. W. Leung, "Wideband circularly polarized dielectric bird-nest antenna with conical radiation pattern," *IEEE Transactions on Antennas and Propagation*, vol. 61, no. 2, pp. 563–570, 2013.

[23] Y. Pan, K. W. Leung, and E. H. Lim, "Compact wideband circularly polarized rectangular dielectric resonator antenna with dual underlaid hybrid couplers," *Microwave and Optical Technology Letters*, vol. 52, no. 12, pp. 2789–2791, 2010.

[24] A. Motevasselian, A. Ellgardt, and B. L. G. Jonsson, "A circularly polarized cylindrical dielectric resonator antenna using a helical exciter," *IEEE Transactions on Antennas and Propagation*, vol. 61, no. 3, pp. 1439–1443, 2013.

[25] S. K. Khamas, "Circularly polarized dielectric resonator antenna excited by a conformal wire," *IEEE Antennas and Wireless Propagation Letters*, vol. 7, pp. 240–242, 2008.

[26] M. D. Yang, Y. M. Pan, and W. J. Yang, "A singly fed wideband circularly polarized dielectric resonator antenna," *IEEE Antennas and Wireless Propagation Letters*, vol. 17, no. 8, pp. 1515–1518, 2018.

[27] J. X. Wen, Y. C. Jiao, Y. X. Zhang, and J. N. Jiai, "Wideband circularly polarized dielectric resonator antenna loaded with partially reflective surface," *International Journal of Microwave and Millimeter-Wave Computer-Aided Engineering*, vol. 29, no. 12, p. e21962, 2019.

[28] L. Wang, "A new broadband circularly polarized dielectric resonator antenna: using parasitic elements," *AEU-International Journal of Electronics and Communications*, vol. 128, 2020.